Assessing theoretical uncertainties in fission barriers of superheavy nuclei

S. E. Agbemava,[1] A. V. Afanasjev,[1] D. Ray,[1] and P. Ring[2]
[1]*Department of Physics and Astronomy, Mississippi State University, Mississippi 39762, USA*
[2]*Fakultät für Physik, Technische Universität München, D-85748 Garching, Germany*
(Received 1 December 2016; revised manuscript received 20 April 2017; published 26 May 2017)

Theoretical uncertainties in the predictions of inner fission barrier heights in superheavy elements have been investigated in a systematic way for a set of state-of-the-art covariant energy density functionals which represent major classes of the functionals used in covariant density functional theory. They differ in basic model assumptions and fitting protocols. Both systematic and statistical uncertainties have been quantified where the former turn out to be larger. Systematic uncertainties are substantial in superheavy elements and their behavior as a function of proton and neutron numbers contains a large random component. The benchmarking of the functionals to the experimental data on fission barriers in the actinides allows reduction of the systematic theoretical uncertainties for the inner fission barriers of unknown superheavy elements. However, even then, on average they increase on moving away from the region where benchmarking has been performed. In addition, a comparison with the results of nonrelativistic approaches is performed in order to define full systematic theoretical uncertainties over the state-of-the-art models. Even for the models benchmarked in the actinides, the difference in the inner fission barrier height of some superheavy elements reaches 5–6 MeV. This uncertainty in the fission barrier heights will translate into huge (many tens of the orders of magnitude) uncertainties in the spontaneous fission half-lives.

DOI: 10.1103/PhysRevC.95.054324

I. INTRODUCTION

The region of superheavy elements (SHE), characterized by the extreme values of proton number Z, is one of the extremes of the nuclear landscape and an arena of active experimental and theoretical studies (see Refs. [1–3] and references therein). Contrary to other regions of the nuclear chart, the SHE are stabilized only by quantum shell effects. Currently available experimental data reach proton number $Z = 118$ [4,5] and dedicated experimental facilities such as the Dubna Superheavy Element Factory will hopefully allow to extend the region of SHE up to $Z = 120$ and for a wider range of neutron numbers for lower Z values.

The stability of SHEs is defined by the fission barriers. In addition, the experimental studies of SHEs are based on the observation of α decays. As a consequence, only SHEs with spontaneous fission half-lives τ_{SF} longer than the half-lives τ_α of the α decays could be observed in experiments. An additional limit is set up by the fact that only α decays longer than 10 μs can be observed in experiment. Therefore, it is of great importance to study the fission barriers in SHEs. The height of the fission barrier, B_f, which is the difference of the energies of the respective saddle in the potential energy surface (PES) and the ground state, is one of most important quantities. It defines the survival probability of SHEs synthesized in heavy-ion reactions and impacts the spontaneous fission half-lives. The latter is important for an understanding of the competition between the fission process and α-particle emission.

Fission barriers have been extensively studied in different theoretical frameworks; these studies have been reviewed in Refs. [1,6]. The theoretical frameworks used are the microscopic + macroscopic method [7], nonrelativistic density functional theories (DFT) based on finite-range Gogny [8] and zero-range Skyrme forces [9], and covariant density functional theory (CDFT) [10]. Our present investigation is performed in CDFT. It has been less frequently used in the studies of fission barriers in SHEs as compared with nonrelativistic theories: a systematic investigation of the fission barriers in the $Z = 112$–120 SHE has been performed in the triaxial relativistic mean field plus BCS (RMF + BCS) framework with the NL3* functional in Ref. [11] and potential energy surfaces in the (β,γ) plane for the even-even isotopes in the α-decay chains of the $^{298}120$ and $^{300}120$ nuclei have been calculated in the triaxial relativistic Hartree-Bogoliubov approach with the DD-PC1 functional in Ref. [12].

Theoretical investigations require an estimate of theoretical uncertainties. This becomes especially important when one deals with the extrapolations beyond the known regions, as, for example, in particle number or deformation. This issue has been discussed in detail in Refs. [13,14] and in the context of global studies within CDFT in the introduction of Ref. [15]. In the CDFT framework, the studies of theoretical uncertainties have been restricted to the ground-state properties so far. Systematic theoretical uncertainties and their sources have been studied globally for the ground-state masses, deformations, charge radii, neutrons skins, positions of drip lines, etc., in Refs. [3,15–19]. Of particular importance in the context of the present paper is the study of theoretical uncertainties in the ground-state properties of SHE presented in Ref. [3]. An analysis of statistical theoretical uncertainties in the ground-state observables is currently under way and will be submitted for publication soon [20]. The major goal of the present paper is to extend these investigations to excited states, namely, to the fission barriers in superheavy nuclei. Both statistical and systematic theoretical uncertainties in the description of fission barriers will be considered here.

Theoretical uncertainties emerge from the underlying theoretical approximations. In the DFT framework, there are two major sources of these approximations, namely, the range of interaction and the form of the density dependence of the effective interaction [9,21]. In the nonrelativistic case, one has zero-range Skyrme and finite-range Gogny forces and different density dependencies [9]. A similar situation exists also in the relativistic case: Point coupling and meson exchange models have interactions of zero and finite range, respectively [10,22–24]. The density dependence is introduced either through an explicit dependence of the coupling constants [22,24,25] or via nonlinear meson couplings [21,23]. This ambiguity in the definition of the range of the interaction and its density dependence leads to several major classes of the covariant energy density functionals (CEDF), which were discussed in Ref. [15].

As a consequence, in the present paper, we focus on the uncertainties related to the choice of the energy density functional. They can be relatively easily deduced globally [15] (at least for axial reflection symmetric shapes). We therefore define theoretical uncertainty for a given physical observable (which we call in the following "spreads") via the spread of theoretical predictions as [15]

$$\Delta O(Z,N) = |O_{\max}(Z,N) - O_{\min}(Z,N)|, \qquad (1)$$

where $O_{\max}(Z,N)$ and $O_{\min}(Z,N)$ are the largest and smallest values of the physical observable $O(Z,N)$ obtained within the set of CEDFs under investigation for the (Z,N) nucleus. Note that these spreads are only a crude approximation of the *systematic* theoretical errors discussed in Ref. [14] since they are obtained with a very small number of functionals which do not form an independent statistical ensemble. Note also that these *systematic* errors are not well defined in unknown regions of the nuclear chart or deformation since systematic biases of theoretical models could not be established in these regions in the absence of experimental data and/or an exact theory.

We use the CEDFs NL3* [23], DD-ME2 [22], DD-MEδ [26], DD-PC1 [24], and PC-PK1 [27]. These state-of-the-art functionals represent the essential types of CEDFs used in the literature (for more details, see the discussion in Sec. II of Ref. [15] and the introduction to Ref. [3]). Moreover, their performance and the related theoretical uncertainties have recently been analyzed globally in Refs. [15,18,19,28] and in particular in superheavy nuclei in Ref. [3]. They are characterized by an improved accuracy of the description of experimental data as compared with the previous generation of CEDFs.

In details, they are based on rather different concepts:

(1) NL3* [23], a slightly improved modern version of the well-known functional NL3 [29], is a representative of the first group of CEDFs proposed in 1977 in the pioneering work of Boguta and Bodmer [21]. These two functionals are based on the Walecka model [30] with its three mesons σ, ω, and ρ and include a density dependence through nonlinear meson couplings in the σ channel. In addition to the four basic parameters (m_σ, g_σ, g_ω, and g_ρ), they depend on two nonlinear coupling constants g_2 and g_3 describing the strength of cubic (σ^3) and quartic (σ^4) terms. This class of functionals misses a density dependence in the isovector channel and therefore the asymmetry energy of such functionals is relatively large and their dependence on the density is rather stiff.

(2) The second class of the functionals, originally introduced in 1999 by Typel and Wolter [25], is also based on meson-exchange forces, but the nonlinear meson couplings are replaced by an explicit density dependence of the coupling constants $[g_i(\rho), i = \sigma, \omega, \rho]$ with four additional parameters. The set DD-ME2 [22] is probably one of the most successful CEDFs of this type. Its eight parameters have been adjusted in a very careful way to the binding energies and radii of a set of twelve spherical nuclei. Here, $g_\rho(\rho)$ depends on the density and therefore this set reproduces rather well not only the *ab initio* results for the equation of state (EoS) of symmetric nuclear matter, but also those for neutron matter [31].

(3) The third functional DD-MEδ [26] is in its form very similar to DD-ME2 but it represents a new idea. It is, to a large extent, derived from modern *ab initio* calculations of nuclear matter [32,33]. Therefore, it contains in addition to three mesons σ, ω, and ρ the scalar isovector meson δ. Only four phenomenological parameters (m_σ, g_σ, g_ω, and g_ρ) at saturation density are adjusted to the same set of data as has been used for DD-ME2. All the rest is derived from *ab initio* calculations.

(4) The last two functionals, DD-PC1 [24] and PC-PK1 [27], have been chosen because they represent zero-range functionals, which are technically much simpler than those based on meson exchange forces with finite range. They can be derived in the limit of large meson masses. This class of functionals has been first proposed in the eighties by Manakos *et al.* [34], but only recently their density dependence has been adjusted carefully to experimental data. We chose two versions of this model with a different density dependence and with a different fitting strategy. The functional DD-PC1 [24] contains an exponential density dependence and it has been adjusted only to nuclear matter data and masses of a large set of deformed nuclei. On the other hand, PC-PK1 [27] has a density dependence of polynomial form in all spin-isospin channels and it is adjusted to a very large set of spherical nuclei. Because of its polynomial density dependence, it can also be used for beyond mean field calculations in the framework of the generator coordinate method (GCM) [35]. However, it does not have a density dependence in the isovector channel.

An additional source of theoretical uncertainties is related to the details of the fitting protocol such as the choice of experimental data and the selection of adopted errors. It applies only to a given functional and the related theoretical uncertainties are called *statistical* [14,36]. Note that the selection of adopted errors is to a degree subjective, in

particular, if one deals with quantities of different dimensions. The investigation of statistical theoretical uncertainties for potential energy curves is time-consuming since it involves constrained deformed calculations over a substantial number of grid points performed for a substantial number of the variations of the original functional. As a result, such an analysis is performed only for a single nucleus and only for two CEDFs.

We restrict our investigation to inner fission barriers. There are several reasons behind this choice. A systematic investigation of Ref. [11] within the RMF + BCS framework with the NL3* CEDF has shown that the fission barriers of many SHEs have a double-humped structure in axial reflection-symmetric calculations. The inclusion of octupole and triaxial deformations lowers outer fission barriers by 2 to 4 MeV so that they are only around 2 MeV in height with respect to superdeformed minimum. A similar situation exists also in Gogny DFT calculations [37]. In addition, similar to actinides [38], symmetry unrestricted calculations which combine octupole and triaxial deformations simultaneously could further reduce the heights of outer fission barriers. These low barriers would translate into a high penetration probability for spontaneous fission such that most likely these superdeformed states are metastable and that outer fission barriers do not affect substantially the fission process in total. Note also that outer fission barriers do not exist in most of the SHEs with $Z \geqslant 110$ in Skyrme DFT calculations [39,40]. An accurate description of outer fission barriers would require the use of symmetry unrestricted relativistic Hartree-Bogoliubov (RHB) code. Unfortunately, the computational cost for such an investigation of theoretical uncertainties in the description of outer fission barriers is prohibitively high.

Despite these limitations, this investigation provides for a first time a systematic analysis of theoretical uncertainties in the description of fission barriers within the CDFT framework. It also gives an understanding of which observables and aspects of many-body physics can be predicted with a higher level of confidence than others for density functionals of the given type. Moreover, it is expected that they will indicate which aspects of the many-body problem have to be addressed with more care during the development of the next generation of EDFs. This study also represents an extension of our previous studies of theoretical uncertainties in the global description of the ground-state properties of the nuclei from the proton to neutron drip lines [15–17,19], superheavy nuclei [3], and rotating nuclei [41].

The paper is organized as follows. Section II describes the details of the calculations. The results of global investigation of inner fission barriers and related systematic theoretical uncertainties within the axial RHB framework are discussed in Sec. III. Statistical uncertainties in the description of fission barriers and potential energy curves are investigated in Sec. IV. Section V is devoted to the study of systematic uncertainties in the description of the energies of fission saddles within the triaxial RHB framework. In Sec. VI, we present a comparison of fission barriers obtained in different models. Finally, Sec. VII summarizes the results of our work.

II. NUMERICAL DETAILS

In the present paper, axially symmetric and triaxial RHB frameworks are used for the studies of fission barriers and the related theoretical uncertainties.

First, the axially symmetric RHB framework is used for systematic studies of all $Z = 96$–126 even-even actinides and SHEs from the proton-drip line up to neutron number $N = 196$. The proton-drip lines for the different functionals are defined in Refs. [3,15,16]. The details of this formalism have been discussed in Secs. II–IV of Ref. [15] and Sec. II of Ref. [17]. Thus, we only provide a general outline of the features specific for the current RHB calculations. In these calculations, we solve the RHB equations in an axially deformed oscillator basis [18,42–45]. The truncation of the basis is performed in such a way that all states belonging to the shells up to $N_F = 20$ fermionic shells and $N_B = 20$ bosonic shells are taken into account. As tested in a number of calculations with $N_F = 26$ and $N_B = 26$, this truncation scheme provides sufficient numerical accuracy. For each nucleus, the potential energy curve is obtained in a large deformation range from $\beta_2 = -1.0$ up to $\beta_2 = 1.05$ in steps of $\beta_2 = 0.02$ by means of a constraint on the quadrupole moment Q_{20}. Then, the correct ground-state configuration and its energy are defined; this procedure is especially important for the cases of shape coexistence (see the discussion in Ref. [3]). The effect of the octupole deformation on the binding energies of the ground states (and thus on the heights of inner fission barriers) is also taken into account according to the results obtained in Refs. [18,46]. Note that octupole deformation in the ground states affects fission barriers and their spreads only for the $Z \sim 92$, $N \sim 132$ and $Z \sim 96$, $N \sim 196$ nuclei.

In order to avoid uncertainties connected with the size of the pairing window, we use the separable form of the finite-range Gogny pairing interaction introduced by Tian *et al.* [47]. As follows from the RHB studies with the CEDF NL3* of odd-even mass staggerings, moments of inertia and pairing gaps, the Gogny D1S pairing and its separable form work well in the actinides (Refs. [15,41,48]). A weak dependence of its pairing strength on the CEDF has been observed in the studies of pairing and rotational properties of deformed actinides in Refs. [41,49], of pairing gaps in spherical nuclei in Ref. [15], and of pairing energies in Ref. [17]. Thus, in the present work, the same pairing strength is used also in the calculations with DD-PC1, DD-ME2, DD-MEδ, and PC-PK1. Considering the global character of this study as well as the existing uncertainties in the extrapolation of pairing from actinides (where experimental data could be confronted with the results of calculations) to superheavy nuclei, this is a reasonable choice.

As a next step, we perform triaxial RHB (TRHB) calculations in a parity-conserving Cartesian oscillator basis [45,50] using the same pairing and the same set of the functionals. However, such calculations are enormously time-consuming. Therefore, they cannot be carried out on the same global scale as axial RHB calculations. As a result, we restricted the TRHB studies to a selected set of the $Z = 112$–120 nuclei. These nuclei are located mostly in the region where extensive experimental studies have either been already performed

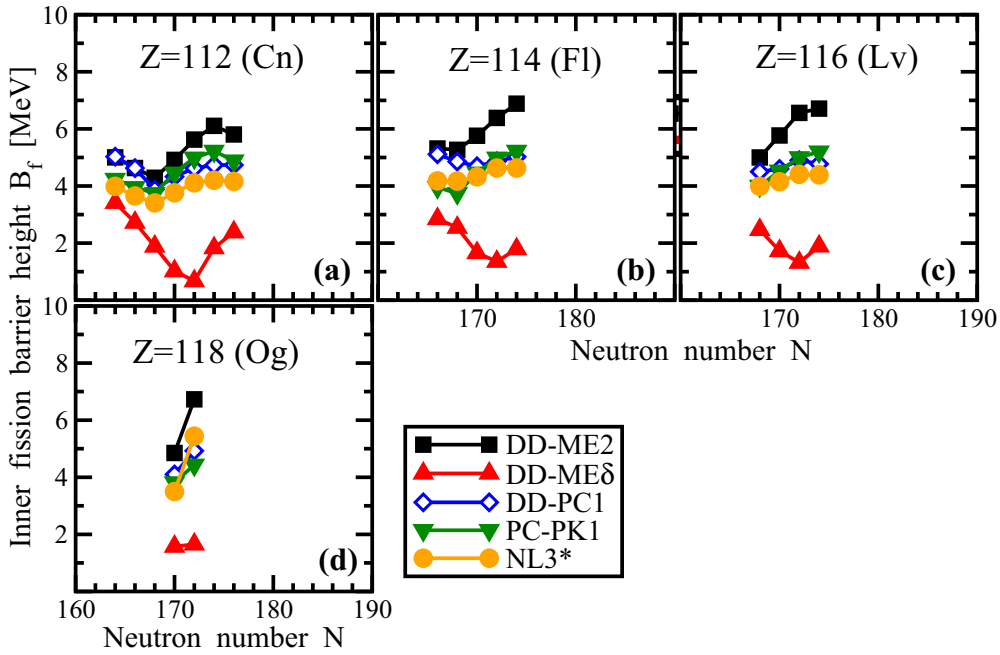

FIG. 1. The heights of inner fission barriers in selected nuclei as obtained in axially symmetric RHB calculations with indicated CEDFs.

or will be performed in a foreseeable future. Even then the calculations of full potential energy surfaces (PES) are numerically prohibitive for the $N_F = 20$ fermionic basis. However, the topology of the PESs obtained in the TRHB calculations with the truncation of the fermionic basis at $N_F = 16$ and $N_F = 20$ is the same. Thus, full PESs have been calculated only with the $N_F = 16$ fermionic basis. These results define the positions in the deformation plane and the energies of axial and triaxial saddles. Afterward, they are corrected for the $N_F = 20$ fermionic basis by performing the TRHB calculations with the $N_F = 20$ fermionic basis in the spherical and normal deformed minimum and at few grid points near the saddles.

III. GLOBAL INVESTIGATION OF INNER FISSION BARRIERS AND RELATED SYSTEMATIC THEORETICAL UNCERTAINTIES IN THE AXIAL RHB CALCULATIONS

Figure 1 compares the heights of inner fission barriers obtained in axially symmetric RHB calculations with the five functionals. We show only results for nuclei in which the lowest saddle is axially symmetric in the systematic triaxial RMF + BCS calculations with NL3* of Ref. [11]. One can see that NL3*, DD-PC1, and PC-PK1, which successfully describe experimental fission barriers in the actinides [11,12,38,51,52], give similar results for the heights of inner fission barriers. On the other hand, the fission barriers produced by DD-ME2 are always at the upper end. This may be a generic feature of this functional since it produces also in ^{236}U and ^{240}Pu inner fission barriers which are higher than those of NL3* and DD-PC1 [11]. The functional DD-MEδ produces unrealistically low fission barriers (see Sec. III in Ref. [11] for a discussion of the inner fission barriers in SHEs).

The global behavior of the inner fission barrier heights in the region of superheavy nuclei is shown in Fig. 2 for all five employed functionals. Again the highest fission barriers are provided by DD-ME2 and the lowest by DD-MEδ.

The employed functionals can be split into two groups [3]. The first group, consisting of NL3*, DD-ME2, and PC-PK1, predicts bands of spherical SHEs in the (Z,N) plane centered around the $Z = 120$ and $N = 184$ lines. The second group includes DD-MEδ and DD-PC1 and it does not predict spherical SHE in the vicinity of the abovementioned particle numbers. The impact of the proton and neutron spherical shell gaps at $Z = 120$ and $N = 184$ is clearly visible for NL3*, DD-ME2, and PC-PK1; there is a substantial increase of the inner fission barrier heights around these numbers. In contrast, no such effect is seen in the calculations with DD-MEδ and DD-PC1. For NL3* and PC-PK1, the heights of the inner fission barriers are lowered around $Z \sim 100$, $N \sim 172$ and $Z \sim 108$, $N \sim 194$. Similar regions of reduced inner fission barrier heights could be found also for the other functionals but they are centered around different combinations of proton and neutron numbers.

The spreads in the predictions of inner fission barrier heights are shown for all five employed functionals in Fig. 3(a). One can see that in the actinides ($Z \leqslant 100, N \leqslant 164$) these spreads are typically smaller than 2.5 MeV. Note that in this mass region theoretical uncertainties in the prediction of the ground-state deformations are very small (see Refs. [3,15]). However, the ΔE^B spreads drastically increase in the $Z = 112$–120, $N = 170$–186 region where they range from 3.5 up to 5.5 MeV. To a large extent, this region coincides with the region where the uncertainties in the predictions of the ground-state deformations are substantial (see Fig. 8 in Ref. [3]). This clearly suggests that in this region the uncertainties in the fission barrier heights are strongly affected

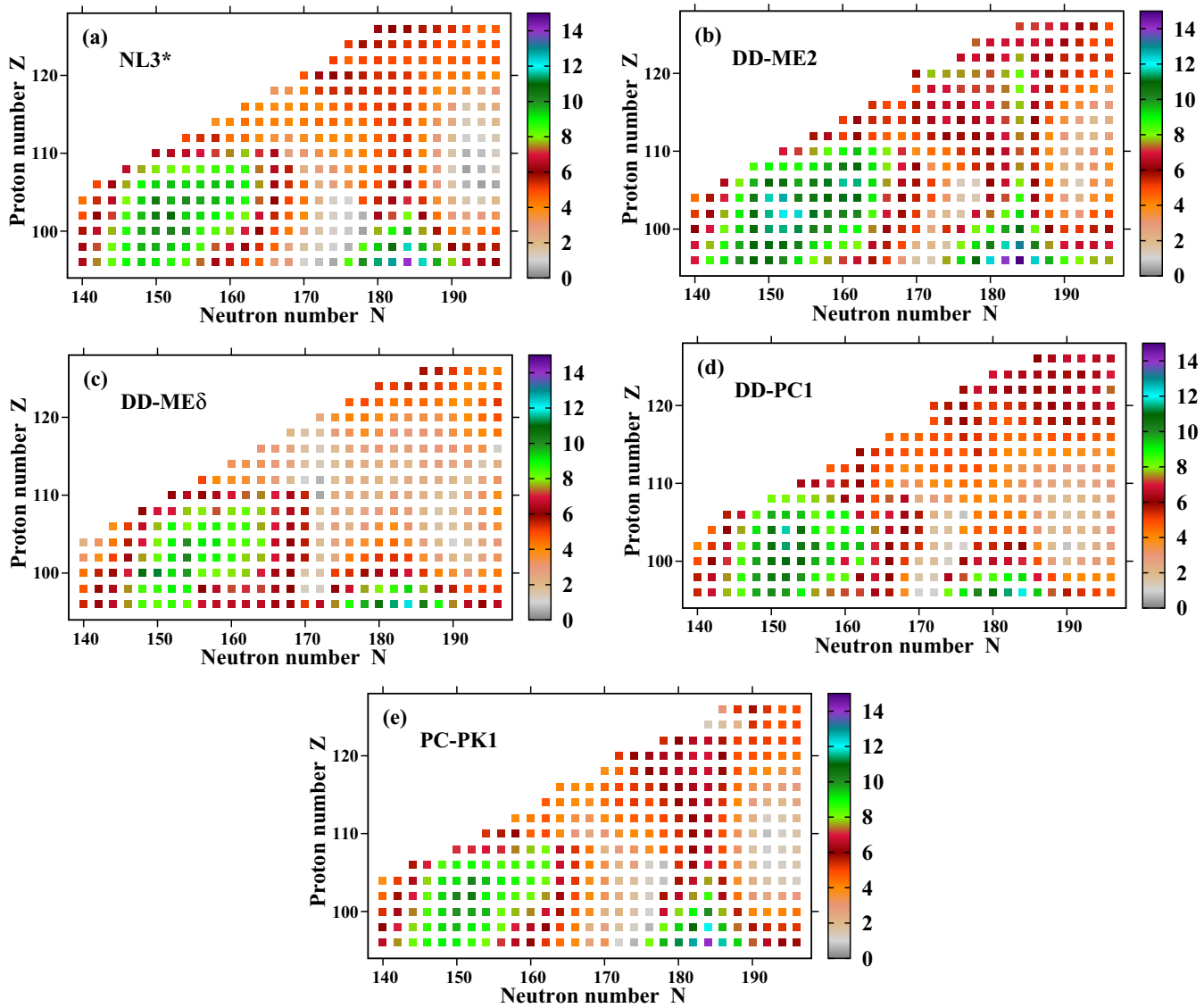

FIG. 2. The heights of inner fission barriers (in MeV) obtained in axially symmetric RHB calculations as a function of proton and neutron numbers. The results of the calculations with the indicated CEDFs are shown from the two-proton drip line up to $N = 196$.

by the uncertainties in the ground-state deformations. A similar enhancement of the ΔE^B spreads is seen in the nuclei around $Z \sim 98$, $N \sim 174$. However, the differences in the predictions of the ground-state deformations play here a minor role since they are almost the same for all functionals (see Fig. 8 in Ref. [3]). Theoretical ΔE^B spreads decrease for $N \geqslant 186$; here they are typically less than 3 MeV with only a few nuclei characterized by higher spreads of around 4 MeV.

The above-discussed impact of the uncertainties in the calculated deformations on the spreads of inner fission barrier heights can be understood in the following way. The inner fission barrier height is the difference between the energies of the saddle and ground states. However, these two points in the potential energy curve have different deformations and thus substantial differences in the underlying shell structure. This leads to different spreads of the binding energies in the ground states and saddles which are compared in Fig. 4. Minimum spreads in these energies appear in the band of the nuclei which is shown in yellow and red colors [Figs. 4(a) and 4(b)]. These spreads increase on going away from this band of the nuclei; this is caused by different isovector properties of employed functionals (see discussion in Ref. [19] for more details). Let focus our discussion on this yellow-red band of the nuclei. Due to different underlying shell structure at the ground state and saddle point, the minima of the spreads (shown by red and reddish colors) in the binding energies are localized in different (Z,N) regions at the ground state and saddle point. Indeed, at the ground state, the increase of the spreads in binding energies takes place near neutron numbers which correspond to the shell gaps in the single-particle spectra, namely, near deformed $N = 162$ shell closure and especially near $N \sim 184$, which corresponds to spherical shell closure in some functionals [Fig. 4(a)]. The situation is different at the saddle point where the increase of the spreads in binding energies appears in wide regions near $N \sim 168$ and $\sim$196 [Fig. 4(b)]. These effects become even more visible when the color map of Fig. 3 is

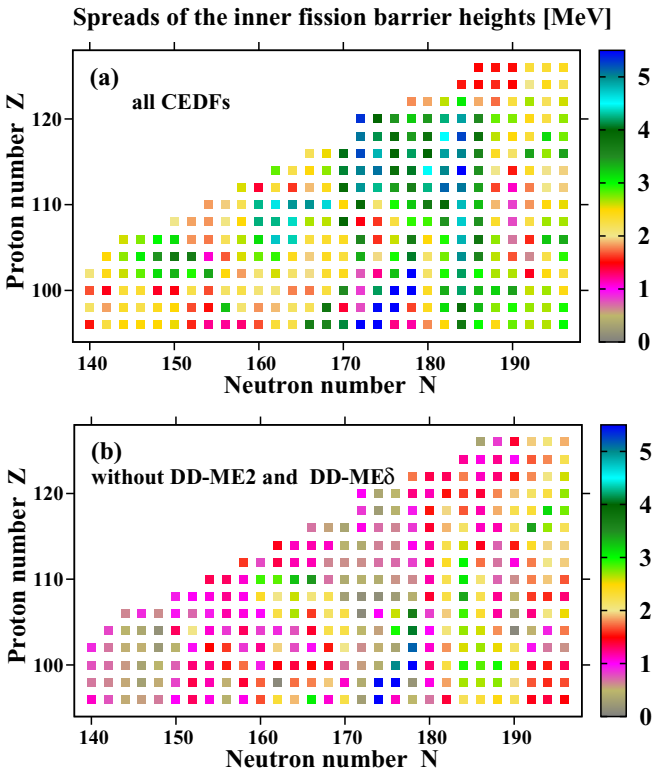

FIG. 3. The spreads ΔE^B of the heights of inner fission barriers as a function of proton and neutron numbers. $\Delta E^B(Z,N) = |E^B_{\max}(Z,N) - E^B_{\min}(Z,N)|$, where, for given Z and N values, $E^B_{\max}(Z,N)$ and $E^B_{\min}(Z,N)$ are the largest and smallest heights of inner fission barriers obtained with the set of functionals NL3*, DD-ME2, DD-MEδ, DD-PC1, and PC-PK1. Panel (a) shows the results for all five functionals, while DD-ME2 and DD-MEδ are excluded in the results shown in panel (b).

used in Figs. 4(c) and 4(d); this is done for simplicity of the comparison of these two figures. The features of the fission barrier spreads which are visible in Fig. 3 (and especially their increase near $N \sim 184$) are consequences of the ones seen in Fig. 4.

The benchmarking of the functionals to experimentally known fission barriers in the actinides allows us to reduce theoretical spreads in their heights for unknown nuclei. This is illustrated in Fig. 3(b), where only the NL3*, DD-PC1, and PC-PK1 functionals are used in the definition of the theoretical spreads. Again, the source of this reduction could be traced back to the reduction of the fluctuations in binding energy spreads for the ground states and saddles in the direction along the direction of minimum spreads (compare Figs. 5 and 4). These functionals successfully describe experimental fission barriers in the actinides [11,12,38,51,52]. One can see that the use of only these functionals reduces theoretical uncertainties in the inner fission barrier heights for the $N \leqslant 180$ nuclei typically to less than 2 MeV; only in few nuclei around $Z = 110, N \sim 164$ and $Z \sim 110, N \sim 176$ do these uncertainties reach 4 and 5.5 MeV, respectively. However, these uncertainties increase by roughly 1 MeV for the nuclei with $N \geqslant 182$. It is also important to mention that theoretical spreads in the inner fission barrier heights do not form a smooth function of proton and neutron numbers; there is always a random component in their behavior.

IV. STATISITICAL UNCERTAINTIES IN THE DESCRIPTION OF FISSION BARRIERS AND POTENTIAL ENERGY CURVES

As discussed in the introduction, there are statistical uncertainties in the description of physical observables in addition to the systematic ones which for the saddles of inner fission barriers are quantified in the previous section and in Secs. V and VI below. The description of the statistical uncertainties for fission barriers and potential energy curves follows the formalism presented in Ref. [14]. Its major details are outlined below.

For a model having $N_{\rm par}$ adjustable parameters $\mathbf{p} = (p_1, p_2, \ldots, p_{N_{\rm par}})$ the normalized objective function is defined as

$$\chi^2_{\rm norm}(\mathbf{p}) = \frac{1}{s} \sum_{i=1}^{N_{\rm type}} \sum_{j=1}^{n_i} \left[\frac{O_{i,j}(\mathbf{p}) - O^{\rm exp}_{i,j}}{\Delta O_{i,j}} \right]^2, \qquad (2)$$

where

$$s = \frac{\chi^2(\mathbf{p}_0)}{N_{\rm data} - N_{\rm par}} \qquad (3)$$

is a global scale factor (Birge factor [53]) defined at the minimum of the penalty function (optimum parametrization $\mathbf{p}_0$), which leads to the average $\chi^2(\mathbf{p}_0)$ per degree of freedom equal to one [14] and

$$N_{\rm data} = \sum_{i=1}^{N_{\rm type}} n_i \qquad (4)$$

is the total number of data points of different types. Here, $N_{\rm type}$ stands for the number of different data types. The calculated and experimental-empirical values of the physical observable j of the ith type are represented by $O_{i,j}(\mathbf{p})$ and $O^{\rm exp}_{i,j}$, respectively. $\Delta O_{i,j}$ is the adopted error for the physical observable $O_{i,j}$.

The acceptable functionals are defined by the condition [14,36]

$$\chi^2_{\rm norm}(\mathbf{p}) < \chi^2_{\rm norm}(\mathbf{p}_0) + 1. \qquad (5)$$

This condition specifies the physically reasonable domain around the minimum $\mathbf{p}_0$ in which the parametrization $\mathbf{p}$ provides a reasonable fit and thus can be considered as acceptable. For a given original functional, the set of the M functional variations $[\mathbf{p}_1, \mathbf{p}_2, \ldots, \mathbf{p}_M]$ has been defined in Ref. [20]; note that this set also includes the original functional.

For this set of the functional variations, the potential energy curves of the $^{296}112$ nucleus have been calculated in the axial RHB framework in the deformation range $\beta_2 = 0.0$–1.05 with a step of $\Delta\beta_2 = 0.02$. Then, the energies of these potential energy curves were redefined with respect of the energy of their spherical or near spherical minimum. As a result, the energy of the minimum becomes equal to zero. Finally, the

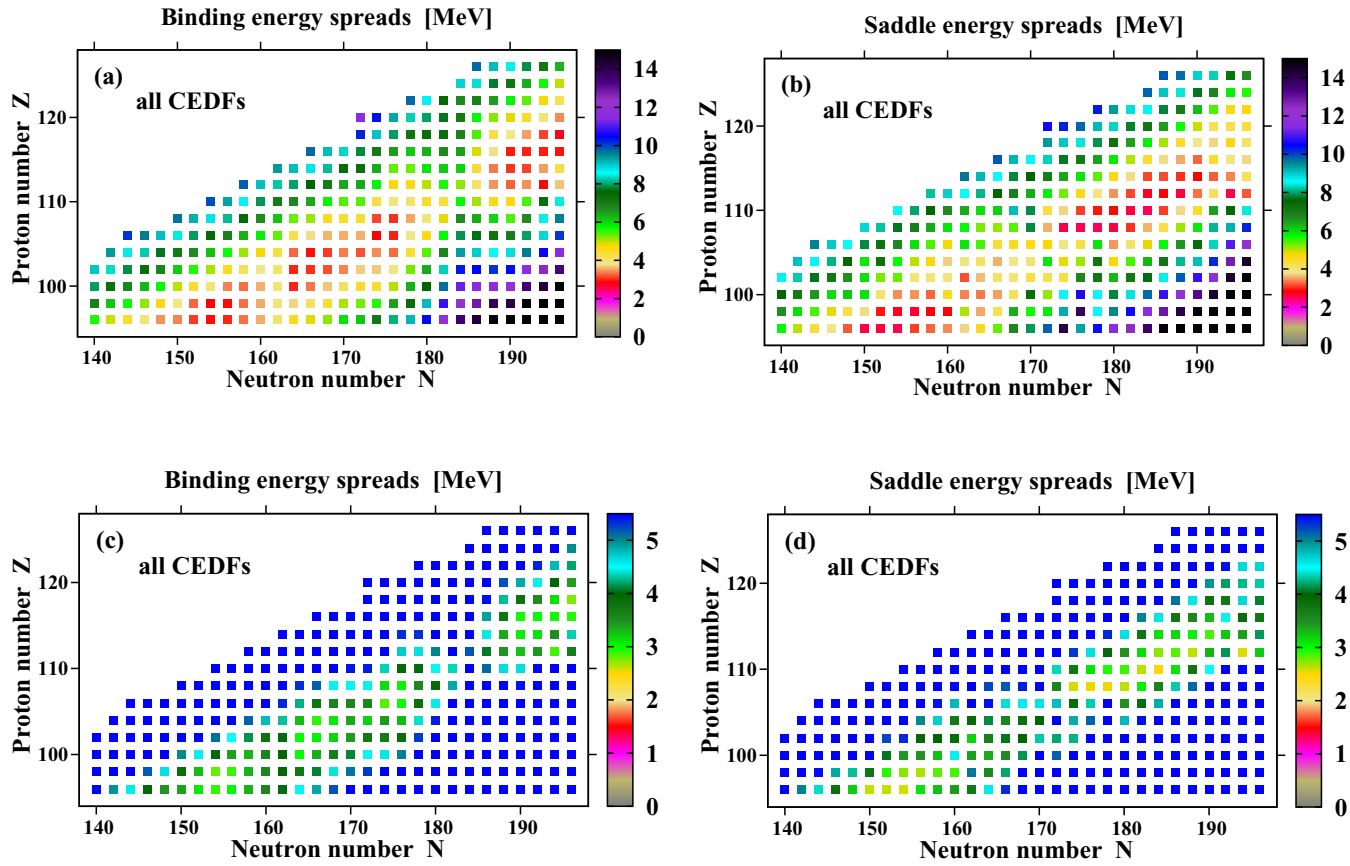

FIG. 4. The spreads in the binding energies of the ground states (a) and the energies of saddle points (b) as obtained with five employed CEDFs. Panels (c) and (d) show the same results but with the energy color map used in Fig. 3.

mean values of the energy

$$\bar{E}(\beta_{2,i}) = \frac{1}{M}\sum_{k=1}^{M} E_k(\beta_{2,i}) \tag{6}$$

and their standard deviations

$$\sigma_E = \sqrt{\frac{1}{M}\sum_{k=1}^{M}[E_k(\beta_{2,i}) - \bar{E}(\beta_{2,i})]^2} \tag{7}$$

have been calculated for this set of potential energy curves at the ith value of the deformation. Note that the standard deviations serve here as a measure of the statistical uncertainty.

The set of the M functional variations defined by the condition of Eq. (5) is represented by 2000 reasonable functionals [20]. Note that they are defined with respect of the ground-state experimental data on 12 spherical nuclei and some empirical data on nuclear matter properties. However, because of numerical restrictions we use the subset of 500 randomly selected functionals in the calculations of potential energy curves and quantities defined in Eqs. (6) and (7). This number of the functionals is sufficient for a reliable definition of the mean values of the energy and their standard deviations. Indeed, the comparison of the results obtained with 250 and 500 functionals reveals very little difference, which strongly suggests that fine details related to statistical properties of the quantities of interest are already imprinted in relatively small number (few hundred) of the functional variations.

The selection of the $^{296}112$ nucleus has been guided by the requirement to avoid large shape changes in the ground state with the variation of the functional. Indeed, this nucleus is spherical in the ground state with a well pronounced minimum in the parabola-like potential energy surface. As a consequence, with exception of a few functional variations, the ground state is spherical in the RHB calculations. On the contrary, larger shape changes in the ground state with the variation of the functional are expected in many nuclei of the region of interest since they are transitional in the ground state with soft potential energy surfaces (see Refs. [3,11]). In such nuclei, statistical theoretical uncertainties in the evolution of the energy with deformation in potential energy curves are expected to be polluted by the variations in the ground-state properties.

Statistical uncertainties in the deformation energy curves are shown in Fig. 6. One can see that in the case of the NL3* functional they are small in the vicinity of the spherical minimum but then increase with increasing deformation. They become especially pronounced in the vicinity of the inner and outer saddles and in the region of the superdeformed (SD) minimum. The σ_E values have a maximum at the inner saddle where they are close to 0.7 MeV. They are smaller at the superdeformed minimum and the outer saddle, where they are close to 0.5 MeV. It is interesting that statistical uncertainties

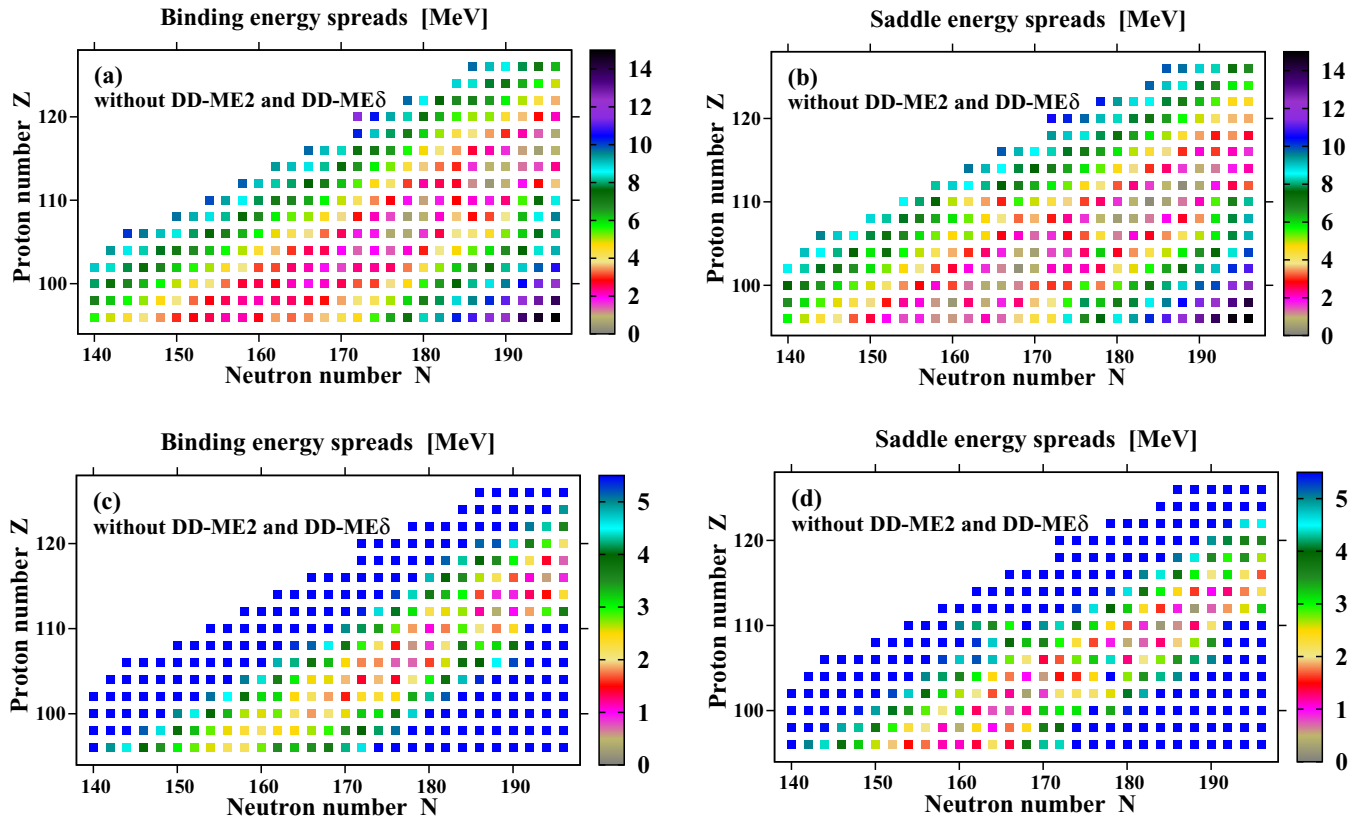

FIG. 5. The same as Fig. 4 but for the case when DD-ME2 and DD-MEδ CEDFs are excluded from consideration.

decrease substantially above the outer fission barrier; here σ_E values are around 0.35 MeV.

Their behavior is quite different for DD-ME2. For this functional, the statistical uncertainties in the deformation range $\beta_2 = 0.0$–0.6 are by approximately factor 1.5 smaller than those obtained with NL3*. However, they increase with increasing deformation and reach a maximum at $\beta_2 \sim 0.85$. With further increase of deformation, they decrease and finally stabilize above $\beta_2 \sim 0.95$.

It is likely that the increased theoretical uncertainties in the region of quadrupole deformations $\beta_2 = 0.1$–0.8 in the case of NL3* and around $\beta_2 \sim 0.85$ in the case of DD-ME2 are due to the underlying single-particle structure. The variations of the functional lead to modifications of the single-particle energies as well as to changes in the sizes of the superdeformed shell gaps and the single-particle level densities at the saddles and the SD minimum. This in turn leads to substantial variations in the shell correction energies. The DD-ME2 functional provides a clear example. Indeed, the increase of statistical uncertainties around $\beta_2 \sim 0.85$ is due to the fact that an additional hump develops in the potential energy curve at this deformation in a number of the functional variations. This fact could only be explained by the underlying shell structure. In addition, the reduced statistical uncertainties at larger deformations and their stabilization strongly support the impact of the underlying single-particle structure on the statistical uncertainties. This is because the shell gaps at hyper- and higher deformations are smaller than at superdeformation (see Refs. [54,55] and references quoted therein). As a consequence, the changes in the single-particle structure caused by the functional variations have a smaller impact on the shell correction energy.

So far, the statistical uncertainties in the deformation energy curves have been investigated only in Skyrme DFT. They have been studied in Ref. [56] for the nucleus ^{240}Pu with the functional UNEDF1 functional and in Ref. [6] for the nucleus ^{266}Hs with the functionals SV-min and SV-bas. In ^{240}Pu, the statistical uncertainties increase on going from the normal deformed minimum to higher deformations and they become especially large after the second fission barrier. The later observation is in contradiction with our results which show a decrease and a stabilization of statistical uncertainties after the second fission barrier. The reasons for such a difference are not clear. They may be related to a different choice of the nuclei. Differences in the analysis also contribute. To avoid the use of the emulator, we restricted our consideration to axially symmetric shapes. On the contrary, the authors of Ref. [56] replace the exact DFT model by a Gaussian process response surface (GPRS) which they "train" to a restricted set of 200 DFT computations. Although this simplified approach allows us to take into account also triaxiality and octupole deformation, it is not clear how well GPRS reproduces the energies for very complicated topologies of the potential energy surfaces (see, for example, Figs. 7 and 8 below) for functional variations not included into the training set. The analysis of ^{266}Hs in Ref. [6] is restricted to the vicinity of the inner fission barrier. Statistical uncertainties obtained with the SV-bas (SV-min) functional are close to (larger than) those obtained in our analysis of ^{296}112.

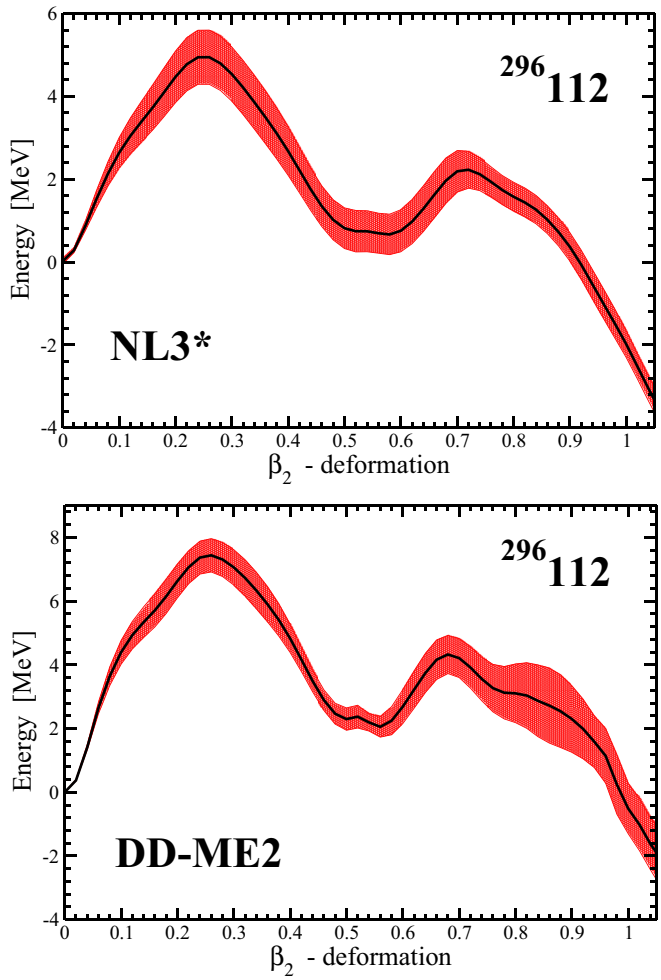

FIG. 6. Statistical uncertainties in the deformation energy curves of the $^{296}112$ nucleus. The mean potential energy curve is shown by a solid line. The red-colored region shows the standard deviations in energy.

V. SYSTEMATIC THEORETICAL UNCERTAINTIES IN THE DESCRIPTION OF INNER FISSION BARRIERS FOR TRIAXIAL RHB CALCULATIONS

Not in all cases is the axial saddle the lowest in energy. The systematic investigation of the heights of inner fission barriers in superheavy nuclei performed within the RMF+BCS approach with the NL3* CEDF in Ref. [11] has revealed that triaxial deformation lowers the heights of the inner fission barriers in a number of nuclei; this is especially pronounced in the vicinity of particle numbers $Z = 120$ and $N = 184$ (see Table V in Ref. [11]). Thus, the axial RHB calculations provide an upper limit for the inner fission barrier heights.

In general, triaxial deformation has to be included into the calculations for a more realistic estimate of the heights of inner fission barriers which can be used for the comparison with experiment. However, such a study requires tremendous computational power. This is also illustrated by the fact that within the covariant and Gogny DFTs, so far only a limited set of superheavy nuclei has been studied in the triaxial Hartree-Bogoliubov framework [12,37,57]. The computational challenge becomes especially large in the case of the analysis of systematic theoretical uncertainties because the same nucleus has to be calculated within the TRHB framework for several CEDFs. Thus, a full global analysis of theoretical uncertainties similar to the one presented in Sec. III in the axial RHB framework is, at present, beyond the reach of available computational facilities. As a result, we concentrate here on the selected set of the $Z = 112$–120 superheavy nuclei which will be in the focus of experimental studies within the next decades. They are shown in Fig. 9 below. In the selection of nuclei we focus on the nuclei in which the triaxial saddle is expected to be the lowest in energy in the region of interest. According to systematic studies in the RMF+BCS framework with the CEDF NL3* of Ref. [11], these are the nuclei in the vicinity of the $Z = 120$ and $N = 184$ lines. On the contrary, the axial saddles are the lowest in energy in the nuclei which are away from these lines. For example, this takes place for $N \leqslant 174$ in the $Z = 112$, 114, 116 nuclei (see Ref. [11]). Triaxial RHB calculations for the ($Z = 112$, $N = 164$), ($Z = 112$, $N = 172$), ($Z = 114$, $N = 166$), and ($Z = 114$, $N = 172$) nuclei [these nuclei are seen on the left side of Fig. 9(a)] confirm this observation of Ref. [11] for all CEDFs employed in the present paper. We will try to establish (i) how theoretical systematic uncertainties obtained in axial RHB calculations will be modified when triaxiality is included and (ii) to what extent theoretical uncertainties obtained in axial and triaxial RHB calculations are correlated.

The dependence of the potential energy surfaces on the CEDF is illustrated in Figs. 7 and 8. These PES are characterized by a complicated topology which, however, reveals some typical triaxial saddles.

For example, in the nucleus $^{300}120$ they are located at ($\beta_2 \sim 0.32$, $\gamma \sim 21^\circ$), ($\beta_2 \sim 0.43$, $\gamma \sim 33^\circ$), and ($\beta_2 \sim 0.49$, $\gamma \sim 24^\circ$) for the functionals DD-ME2, PC-PK1, NL3* and DD-PC1 (see Fig. 7). The later two are also visible in the CEDF DD-MEδ. However, the first one is shifted to smaller β_2 and γ deformations, namely, to ($\beta_2 \sim 0.20$, $\gamma \sim 15^\circ$).

For all functionals except DD-MEδ the axial saddle is higher in energy by roughly 0.5 MeV than the triaxial saddle at ($\beta_2 \sim 0.32$, $\gamma \sim 21^\circ$) and by approximately 1.5 MeV than the triaxial saddles at ($\beta_2 \sim 0.43$, $\gamma \sim 33^\circ$) and ($\beta_2 \sim 0.49$, $\gamma \sim 24^\circ$) (Fig. 7). The PES of the DD-MEδ functional has a completely different topology. Although the ($\beta_2 \sim 0.20$, $\gamma \sim 15^\circ$) saddle is lower in energy than the axial saddle by approximately 1 MeV, the axial saddle is located only $\sim$0.2MeV below the triaxial saddles at ($\beta_2 \sim 0.33$, $\gamma \sim 25^\circ$) and ($\beta_2 \sim 0.45$, $\gamma \sim 33^\circ$).

The presence of these saddles leads to several fission paths which have been discussed in detail in Ref. [11]. Although this discussion is based on RMF + BCS results with NL3*, we found that it is still valid for the TRHB results with DD-ME2, PC-PK1, NL3*, and DD-PC1. This is because for a given functional the topology of PES obtained in triaxial RMF + BCS and RHB calculations is similar. The situation is different for DD-MEδ, which has an axial saddle located at $\beta_2 \sim 0.13$ (Fig. 7). Thus, the fission path will proceed from the oblate minimum via the triaxial saddle at ($\beta_2 \sim 0.20$, $\gamma \sim 0.15$) which has a low excitation energy of only 3 MeV.

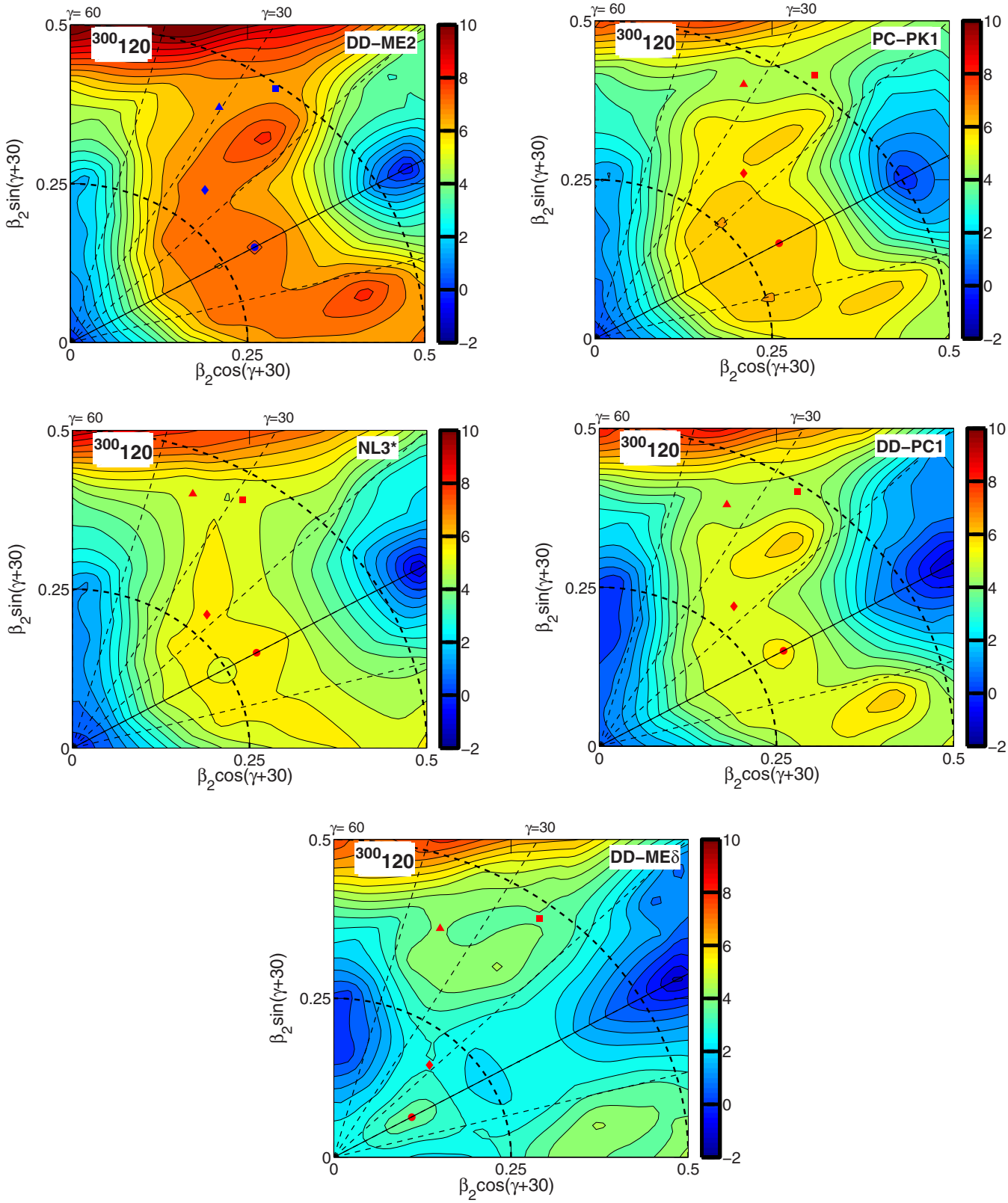

FIG. 7. Potential energy surfaces of the $^{300}120$ nucleus as obtained in the calculations with indicated CEDFs. The energy difference between two neighboring equipotential lines is equal to 0.5 MeV. The Ax, Ax-Tr, Tr-A, and Tr-B saddles are shown by blue or red circles, diamonds, triangles, and squares, respectively. The PES are shown in the order of decreasing height of inner fission barrier.

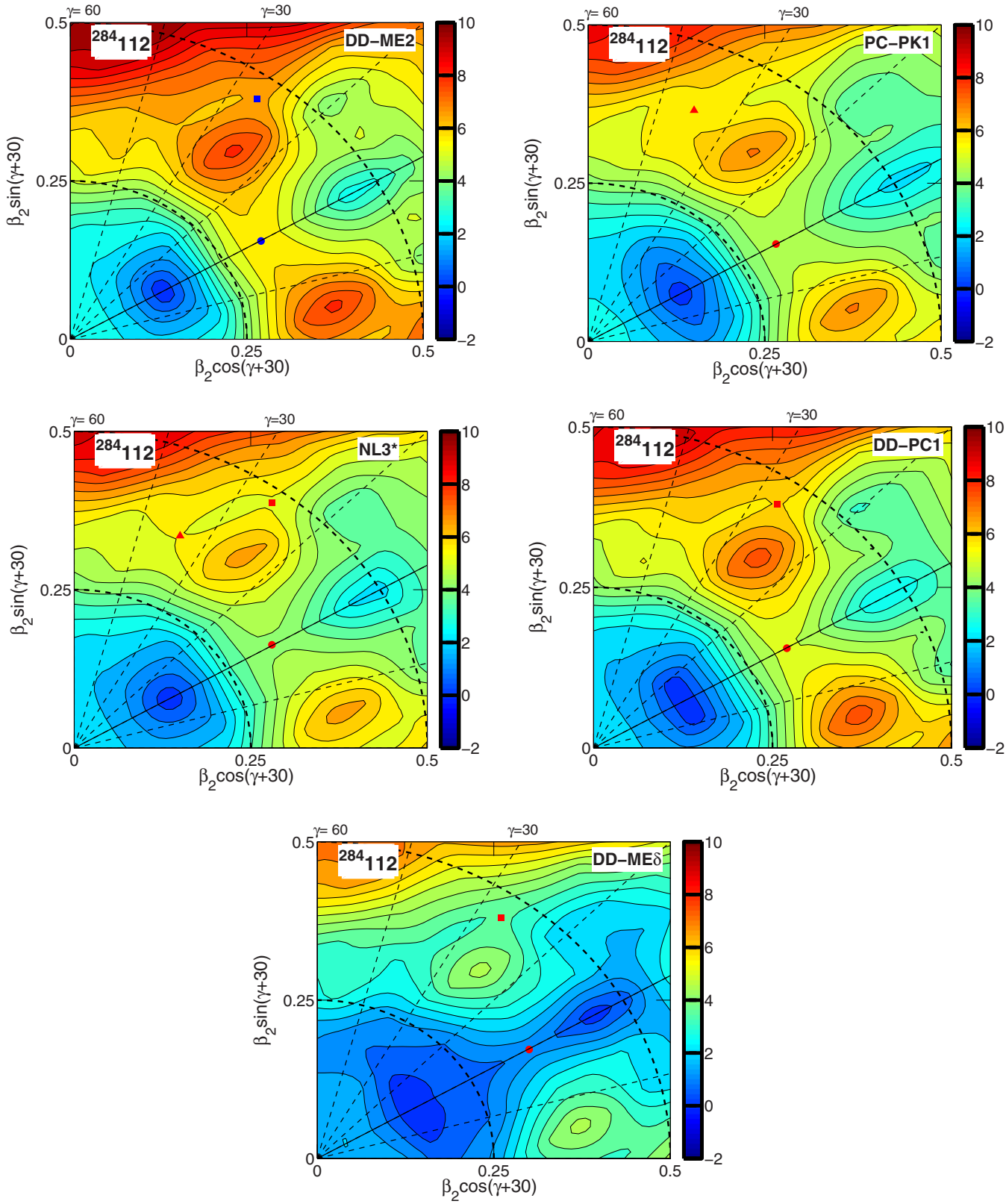

FIG. 8. The same as in Fig. 7 but for the $^{284}112$ nucleus.

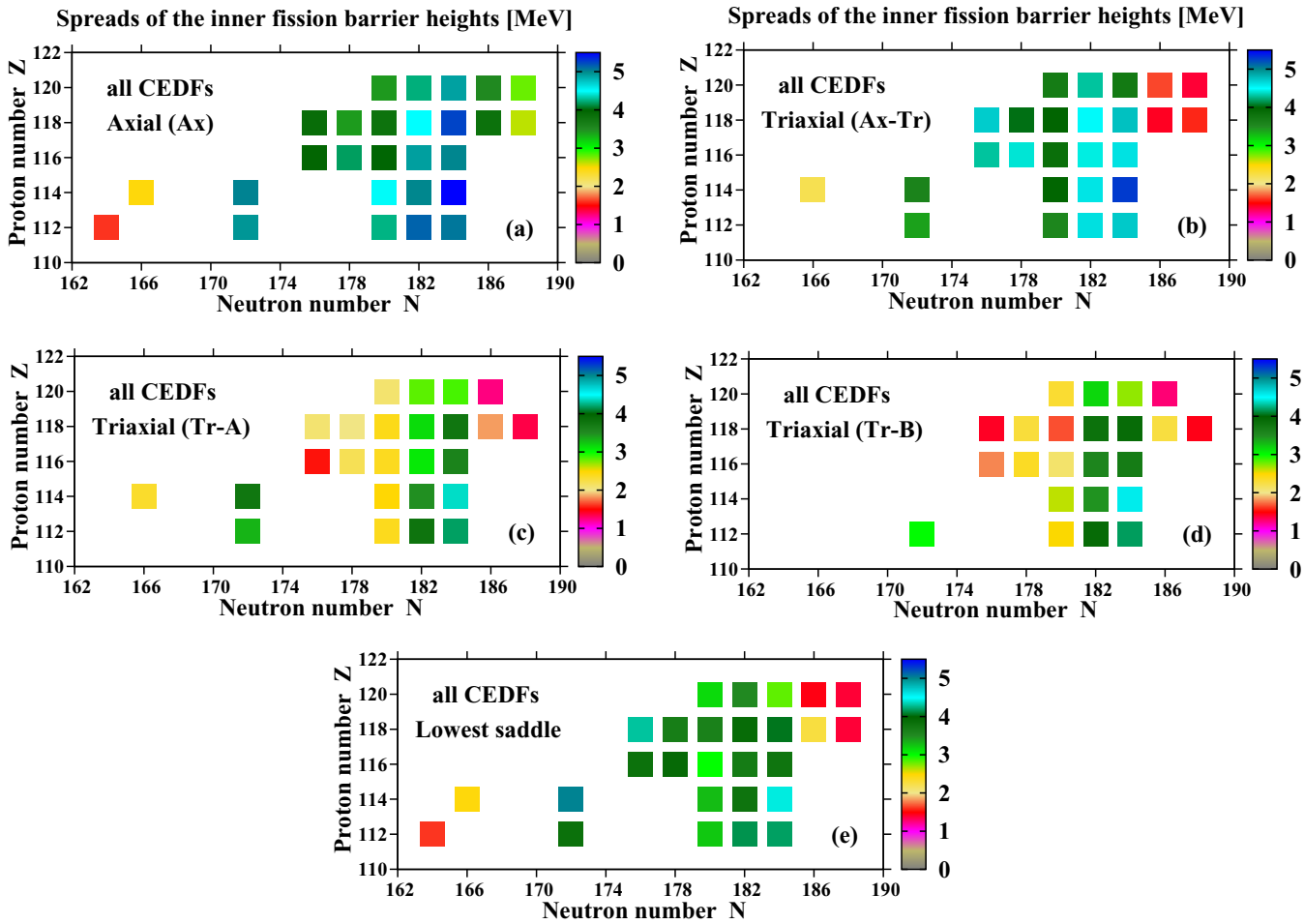

FIG. 9. The spreads ΔE^S of the energies of axial [panel (a)], triaxial [panels (b), (c), (d)], and the lowest in energy [panel (d)] saddles for a selected set of the $Z = 112$–120 nuclei as a function of proton and neutron number. $\Delta E^S(Z,N) = |E^S_{\rm max}(Z,N) - E^S_{\rm min}(Z,N)|$, where, for given Z and N values, $E^S_{\rm max}(Z,N)$ and $E^S_{\rm min}(Z,N)$ are the largest and smallest energies of the saddles obtained with the set of functionals NL3*, DD-ME2, DD-MEδ, DD-PC1, and PC-PK1. Note that the same color map as in Fig. 3 is used here.

As shown in Ref. [11], the axial saddle becomes energetically more favored as compared with triaxial saddles on moving away from the particle numbers $Z = 120$ and $N = 184$. This is clearly seen in the nucleus $^{284}112$, in which the axial saddle at $\beta_2 \sim 0.32$ is lower in energy than the triaxial saddles located around ($\beta_2 \sim 0.38, \gamma \sim 34^\circ$) and ($\beta_2 \sim 0.47, \gamma \sim 26^\circ$). This feature is also seen in Fig. 4 of Ref. [11], which compares the results for selected $Z = 112, 114$, and 116 nuclei obtained in the RMF + BCS calculations with NL3*.

To simplify the further discussion, we follow the notation of Ref. [11] and denote the axial saddle as Ax, the triaxial saddle with ($\beta_2 \sim 0.3, \gamma \sim 10^\circ$) as Ax-Tr, the triaxial ($\beta_2 \sim 0.4, \gamma \sim 35^\circ$) saddle as Tr-A, and the triaxial saddle with ($\beta_2 \sim 0.5, \gamma \sim 22^\circ$) as Tr-B. Although the positions of these saddles move somewhat in the deformation plane with the change of proton and neutron numbers, they appear in the majority of nuclei under study.

Figure 10 summarizes the results of the calculations for the inner fission barrier heights. The DD-ME2 and DD-MEδ functionals provide the highest and the lowest fission barriers among those obtained in the calculations with five CEDFs. The results of the calculations with the CEDFs NL3*, DD-PC1, and PC-PK1 are located in between of these two extremes. Note that these three functionals have been benchmarked in the actinides in Refs. [11,12,38,52], where they provide a good description of experimental data.

Figure 10 clearly shows that different functionals are characterized by different isotopic and isotonic dependencies for the inner fission barrier heights. As a result, the functionals, which give similar results in one part of the (Z,N) plane, could provide substantially different results in another. This leads to the spreads in the predictions of the inner fission barrier heights which are presented in Figs. 9 and 11. The strongest correlation between these spreads is observed for the Ax and Ax-Tr saddles; this is seen both for the set of five [Figs. 9(a) and 10(b)] and the set of three [Figs. 11(a) and 11(b)] functionals. This is because these saddles are closely located in the deformation plane so that the change in the energy of the Ax saddle affects in a similar way the energy of the Ax-Tr saddle. The correlations in the spreads of the energies of the Ax saddle on one hand and the Tr-A and Tr-B saddles, on the other hand,

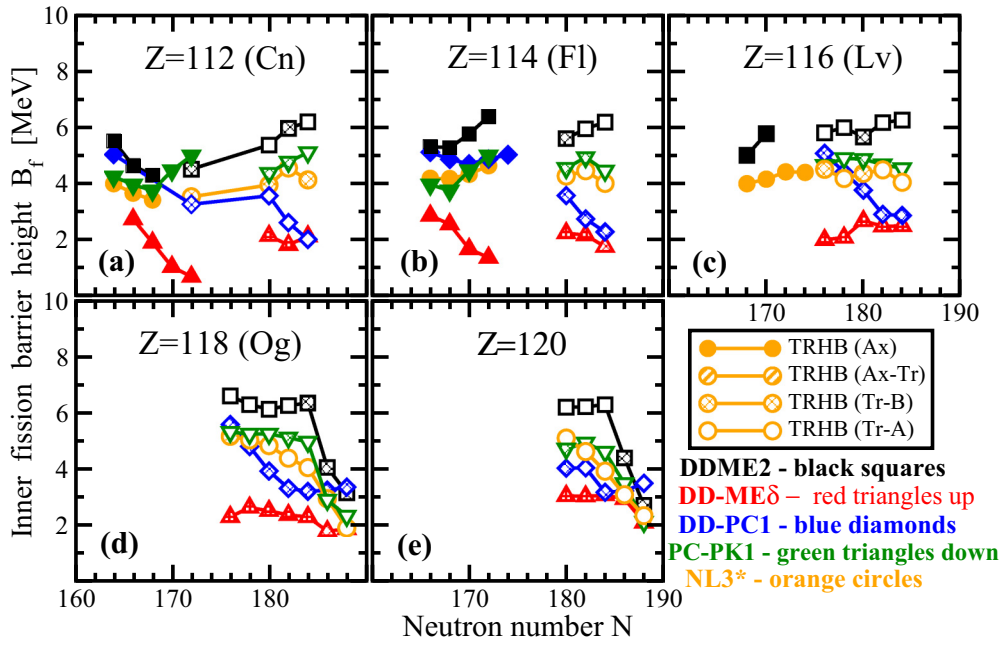

FIG. 10. The heights of inner fission barriers in selected nuclei as obtained in the TRHB calculations with indicated CEDFs. The style of the symbol filling indicates the type of the lowest in energy saddle. Note that the TRHB results in a few $N \sim 166$ and $N = 172$ nuclei (see Fig. 9 below) and the trends of the evolution of PES with particle number allow us to firmly establish the axially symmetric nature of the lowest saddle in the $Z = 112$ and 114 nuclei (as well as in $Z = 116$ nuclei for the NL3* and DD-ME2 functionals) for neutron numbers between 164 and approximately $N = 172$. For some of these nuclei, we use axial RHB results when the TRHB results are not available.

depend on how many functionals are used in the analysis. On average, they are strongly correlated for the set of the DD-PC1, NL3*, and PC-PK1 functionals [compare Figs. 11(a), 11(c), and 11(d)], which have large similarities in the topology of PESs (see Figs. 7 and 8) and for which the ΔE^S spreads are typically below 2 MeV (see Fig. 11). Note that these three functionals successfully describe experimental fission barriers in the actinides [12,51,52]. These correlations decrease with the addition of the functionals DD-MEδ and DD-ME2; the ΔE^s spreads are typically smaller for the Tr-A and Tr-B saddles as compared with the Ax one [compare Figs. 9(a), 10(c), and 10(d)].

It is important that the spreads for the axial Ax saddles and the lowest in energy saddles are strongly correlated [compare Figs. 9(a) and 10(d) and Figs. 11(a) and 11(d)]. This suggests that also for other regions of nuclear chart, not covered by the present TRHB calculations, the spreads in inner fission barrier heights obtained in the axial RHB calculations could be used as a reasonable estimate of the spreads which would be obtained in the calculations with triaxiality included.

VI. COMPARISON OF FISSION BARRIERS IN DIFFERENT MODELS

It is necessary to recognize that the CDFT represents only one of the classes of nuclear structure models. Other classes are represented by nonrelativistic DFTs based on zero-range Skyrme and finite-range Gogny forces as well as microscopic + macroscopic approaches based on phenomenological folded Yukawa and Woods-Saxon potentials. As can be seen for instance in Refs. [11,58], these models accurately reproduce the inner fission barriers in the actinides. This is in part due to the fact that the heights of fission barriers and/or the energy of the fission isomers have been used in their fitting protocols.

Thus, it is important to understand how these models extrapolate to the edge on the known region of superheavy nuclei and its vicinity. This is because the differences in their predictions define the systematic uncertainties. Figure 12 shows the heights of inner fission barriers of the $Z = 112$–120 superheavy nuclei for various relativistic and nonrelativistic models. While providing similar predictions in the actinides, they do extrapolate in very different ways to the superheavy region. Their predictions vary significantly and the inner fission barrier heights found within these models can differ by up to 6 MeV. The substantial differences in the predictions of the two macroscopic + microscopic (MM) are in particular surprising. Unfortunately, at present, there are only very few experimental data available on fission barriers in superheavy elements and they are not reliable enough to distinguish between theoretical predictions of the various models (see discussion in Ref. [11]).

Figure 12 also compares the energies of the lowest inner fission barriers obtained in triaxial RMF + BCS (Ref. [11]) and RHB (present paper) calculations with the CEDF NL3*. Pairing correlations are treated in these two calculations in a very different way. Monopole pairing with a finite pairing window is used in the RMF + BCS calculations of Ref. [11]. Its strength is adjusted to the empirical pairing gaps of Ref. [61]. In the RHB calculations, the separable form of the finite-range Gogny pairing interaction [47] is used. As discussed in Sec. II, this pairing well reproduces physical observables sensitive to pairing in the actinides. The differences in the calculated inner

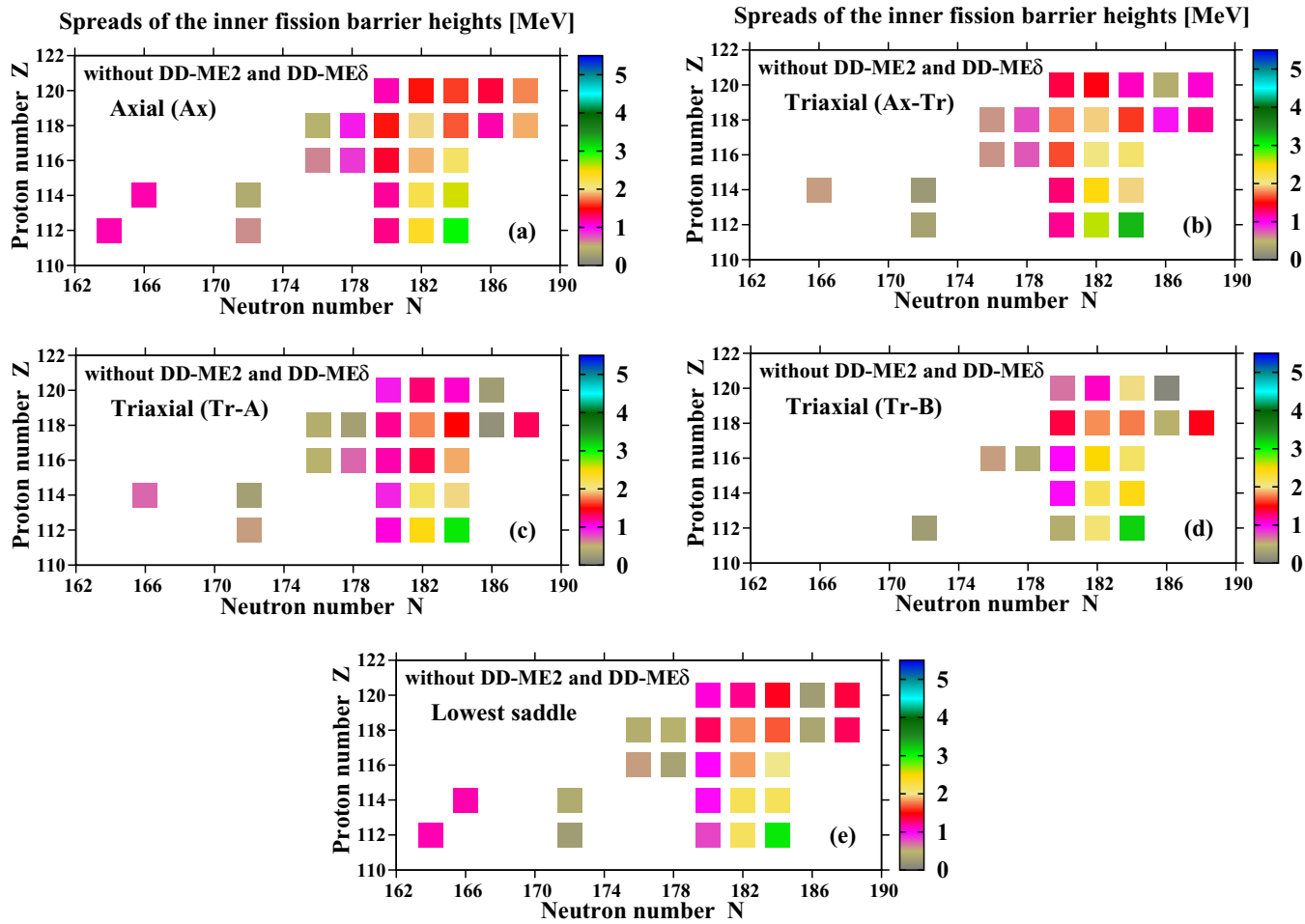

FIG. 11. The same as in Fig. 9 but for the case when the DD-ME2 and DD-MEδ CEDFs are excluded from consideration.

fission barriers seen in Fig. 12 are (i) due to different extrapolation properties of these two types of pairing on going from actinides to the superheavy region and (ii) due to the dependence of fission barrier heights on the pairing window used for the monopole force [62]. Because of these reasons the inner fission barriers are found to be roughly 1 MeV higher in the RHB results than in the RMF+BCS calculations for $N \leqslant 174$ ($N > 176$). For these neutron numbers, the RHB results come closer to the mic-mac model predictions MM (Kowal). However, the difference between the TRHB and RMF + BCS results decreases at higher N. Note that for the $Z = 118$ and 120 nuclei the TRHB results are close to the MM (Kowal) results.

Of course, it is very difficult to measure the fission barriers. On the other hand, one can consider also the spontaneous fission half-lives τ_{SF}, which are directly measurable quantities. Their calculations, however, represent a real challenge. The values of spontaneous fission half-lives depend strongly on the underlying theory used to describe the collective motion, such as the generator coordinate method (GCM) or the adiabatic time-dependent HFB (ATDHFB) theory (for details, see Refs. [63,64]) and the corresponding collective Hamiltonian, in particular, on the inertia parameters. Typical differences between the τ_{SF} values calculated with ATDHFB and GCM can reach many orders of magnitude [65].

In addition, the uncertainties (both systematic and statistical) in the calculated heights of inner fission barriers discussed above will also have a profound effect on the calculated spontaneous fission half-lives. For example, it is well known that the change of fission barrier height by 1 MeV leads to a change of the calculated spontaneous fission half-lives τ_{SF} by 6 orders of magnitude [65]. It is more difficult to quantify the impact of the change of the topology of the PES on τ_{SF}, but it is reasonable to expect that it is substantial.

As a result, the absolute values of calculated spontaneous fission half-lives τ_{SF} cannot be used with confidence since they have extremely large theoretical uncertainties spanning many orders of magnitude. However, it is frequently argued that isotopic and/or isotonic trends in the description of spontaneous half-lives are expected to be reproduced with much higher accuracy [65]. However, such arguments are usually based on a single functional. On the contrary, the current analysis based on a set of the state-of-the art CEDFs as well as the comparison with other models shown in Fig. 12 indicates substantial theoretical uncertainties in isotopic and isotonic trends for the inner fission barriers, even for the functionals which are benchmarked in the actinides. In addition, these uncertainties have a chaotic component which randomly changes from nucleus to nucleus. These uncertainties will

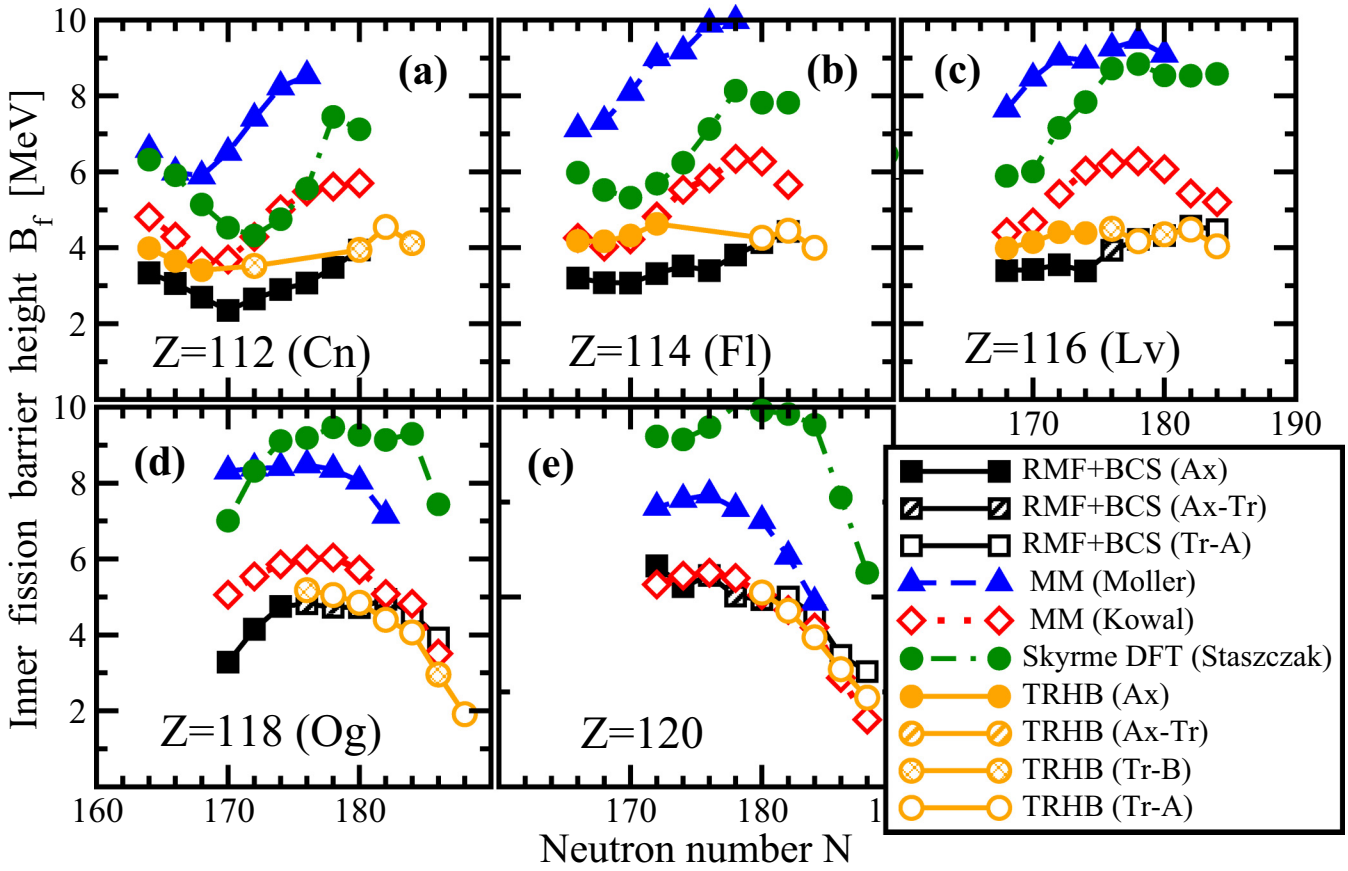

FIG. 12. Inner fission barrier heights B_f as a function of the neutron number N. The position of the inner fission barrier saddle in deformation space varies as a function of particle number. Thus, the lowest saddles are labeled by Ax, Ax-Tr, Tr-A, and Tr-B (see text for details). The results of triaxial RMF + BCS calculations are taken from Ref. [11]. The results of Skyrme DFT calculations with SkM* have been taken from Ref. [40]. The results of the MM calculations are taken from Ref. [59] [labeled as MM (Möller)] and Ref. [60] [labeled as MM (Kowal)]. Note that the style of Fig. 1 is used here for easy comparison between two figures.

definitely affect the calculated spontaneous fission half-lives by many orders of magnitude. This fact is important not only for our understanding of SHEs but also for fission recycling in neutron star mergers [66]. The latter process will be definitely affected by the increased (as compared with the actinides) uncertainties of the inner fission barrier heights seen in neutron-rich nuclei (see Fig. 3).

VII. CONCLUSIONS

Theoretical uncertainties in the predictions of inner fission barrier heights in SHEs have been investigated for the first time in a systematic way for covariant energy density functionals. The analysis is based on the state-of-the-art functionals NL3*, DD-ME2, DD-MEδ, DD-PC1, and PC-PK1 which represent major classes of CEDFs with different basic model assumptions and fitting protocols. These functionals have been used earlier in the assessment of theoretical uncertainties in the description of various ground-state observables in Refs. [3,15,16,18,20]. The following results have been obtained:

(1) Systematic theoretical uncertainties in the predictions of inner fission barriers and their propagation towards unknown regions of higher Z values and of more neutron-rich nuclei have been quantified. These uncertainties are substantial in SHEs. Statistical uncertainties are smaller than systematic ones. It is clear that the differences in the basic model assumptions such as a range of the interaction and the form of the density dependence together with the different fitting protocols based only on nuclear matter and bulk properties data lead to these uncertainties.

(2) Systematic theoretical uncertainties in the inner fission barrier heights do not form a smooth function of proton and neutron numbers; there is always a random component in their behavior. This is a consequence of the fact that fission barrier height is the difference of the energies between the ground state and saddle point. Any differences in the predictions of their energies, which are not acting coherently as a function of proton and neutron numbers, will lead to this random component.

(3) Benchmarking of the functionals to the experimental data on fission barriers in the actinides allows us to reduce the theoretical uncertainties for the inner fission barriers of unknown SHEs. However, even

then they increase on moving away from the region where benchmarking has been performed. This feature is seen not only for different CEDFs but also for different classes of the models such as microscopic + macroscopic and nonrelativistic DFTs. The resulting uncertainties in the heights of inner fission barriers will result in uncertainties of many orders of magnitude for spontaneous fission half-lives. The increased theoretical uncertainties in the fission barriers of neutron-rich SHEs could have a substantial impact on fission recycling modeling in r-process simulations of neutron-star mergers.

(4) Comparing different functionals, one can see that the results (including the topology of the PES) obtained with DD-MEδ differ substantially from the results of other functionals. The heights of the inner fission barriers obtained with this functional are significantly lower than the experimental estimates in the $Z = 112$–116 nuclei and the values calculated in all other models. In addition, this functional does not lead to octupole deformation in those actinides, which are known to be octupole deformed [18]. Thus, this functional is not recommended for future investigations in the actinides and superheavy nuclei in spite of the fact that it provides a good description of masses and other ground-state observables in the $Z \leqslant 82$ nuclei [15].

The analysis of the description of fission barrier heights is frequently performed in terms of the parameters which are related to bulk properties (see, for example, the discussion in Ref. [6]). However, this is only part of the physics which affects the heights of fission barriers. Indeed, it is well known that in actinides the lowering of the inner and outer fission barriers due to triaxial and octupole deformations is caused by relevant changes in the single-particle density which affect the shell correction energy [11,59]. Substantial differences in the predictions of the ground-state deformations by the state-of-the-art CEDFs along the $Z = 120$ and $N = 184$ lines (see Ref. [3]) are also caused by the differences in the underlying single-particle structure. The differences among the models in the single-particle structure of superheavy nuclei are substantially higher than in the region of known nuclei [3,67]. It is clear that this is one of the major contributors to the systematic theoretical uncertainties in the description of inner fission barriers. A further improvement in the description of the single-particle energies within DFT is needed in order to reduce the systematic theoretical uncertainties in the description of fission barriers.

ACKNOWLEDGMENTS

This material is based upon work supported by the Department of Energy National Nuclear Security Administration under Award No. DE-NA0002925, by the US Department of Energy, Office of Science, Office of Nuclear Physics under Award No. DE-SC0013037, and by the DFG cluster of excellence "Origin and Structure of the Universe" (www.universe-cluster.de).

[1] A. Sobiczewski and K. Pomorski, Prog. Part. Nucl. Phys. **58**, 292 (2007).
[2] Y. T. Oganessian and V. K. Utyonkov, Rep. Prog. Phys. **78**, 036301 (2015).
[3] S. E. Agbemava, A. V. Afanasjev, T. Nakatsukasa, and P. Ring, Phys. Rev. C **92**, 054310 (2015).
[4] Y. T. Oganessian, V. K. Utyonkov, Y. V. Lobanov, F. S. Abdullin, A. N. Polyakov, R. N. Sagaidak, I. V. Shirokovsky, Y. S. Tsyganov, A. A. Voinov, G. G. Gulbekian, S. L. Bogomolov, B. N. Gikal, A. N. Mezentsev, S. Iliev, V. G. Subbotin, A. M. Sukhov, K. Subotic, V. I. Zagrebaev, G. K. Vostokin, M. G. Itkis, K. J. Moody, J. B. Patin, D. A. Shaughnessy, M. A. Stoyer, N. J. Stoyer, P. A. Wilk, J. M. Kenneally, J. H. Landrum, J. F. Wild, and R. W. Lougheed, Phys. Rev. C **74**, 044602 (2006).
[5] Y. T. Oganessian, F. S. Abdullin, C. Alexander, J. Binder, R. A. Boll, S. N. Dmitriev, J. Ezold, K. Felker, J. M. Gostic, R. K. Grzywacz, J. H. Hamilton, R. A. Henderson, M. G. Itkis, K. Miernik, D. Miller, K. J. Moody, A. N. Polyakov, A. V. Ramayya, J. B. Roberto, M. A. Ryabinin, K. P. Rykaczewski, R. N. Sagaidak, D. A. Shaughnessy, I. V. Shirokovsky, M. V. Shumeiko, M. A. Stoyer, N. J. Stoyer, V. G. Subbotin, A. M. Sukhov, Y. S. Tsyganov, V. K. Utyonkov, A. A. Voinov, and G. K. Vostokin, Phys. Rev. Lett. **109**, 162501 (2012).
[6] A. Baran, M. Kowal, P.-G. Reinhard, L. M. Robledo, A. Staszczak, and M. Warda, Nucl. Phys. A **944**, 442 (2015).
[7] S. G. Nilsson and I. Ragnarsson, *Shapes and Shells in Nuclear Structure* (Cambridge University Press, Cambridge, UK, 1995).
[8] S. Peru and M. Martini, Eur. Phys. J **50**, 88 (2014).
[9] M. Bender, P.-H. Heenen, and P.-G. Reinhard, Rev. Mod. Phys. **75**, 121 (2003).
[10] D. Vretenar, A. V. Afanasjev, G. A. Lalazissis, and P. Ring, Phys. Rep. **409**, 101 (2005).
[11] H. Abusara, A. V. Afanasjev, and P. Ring, Phys. Rev. C **85**, 024314 (2012).
[12] V. Prassa, T. Nikšić, G. A. Lalazissis, and D. Vretenar, Phys. Rev. C **86**, 024317 (2012).
[13] P. G. Reinhard and W. Nazarewicz, Phys. Rev. C **81**, 051303(R) (2010).
[14] J. Dobaczewski, W. Nazarewicz, and P.-G. Reinhard, J. Phys. G **41**, 074001 (2014).
[15] S. E. Agbemava, A. V. Afanasjev, D. Ray, and P. Ring, Phys. Rev. C **89**, 054320 (2014).
[16] A. V. Afanasjev, S. E. Agbemava, D. Ray, and P. Ring, Phys. Lett. B **726**, 680 (2013).
[17] A. V. Afanasjev, S. E. Agbemava, D. Ray, and P. Ring, Phys. Rev. C **91**, 014324 (2015).
[18] S. E. Agbemava, A. V. Afanasjev, and P. Ring, Phys. Rev. C **93**, 044304 (2016).
[19] A. V. Afanasjev and S. E. Agbemava, Phys. Rev. C **93**, 054310 (2016).
[20] A. V. Afanasjev and S. E. Agbemava (unpublished).
[21] J. Boguta and R. Bodmer, Nucl. Phys. A **292**, 413 (1977).
[22] G. A. Lalazissis, T. Nikšić, D. Vretenar, and P. Ring, Phys. Rev. C **71**, 024312 (2005).

[23] G. A. Lalazissis, S. Karatzikos, R. Fossion, D. P. Arteaga, A. V. Afanasjev, and P. Ring, Phys. Lett. B **671**, 36 (2009).
[24] T. Nikšić, D. Vretenar, and P. Ring, Phys. Rev. C **78**, 034318 (2008).
[25] S. Typel and H. H. Wolter, Nucl. Phys. A **656**, 331 (1999).
[26] X. Roca-Maza, X. Viñas, M. Centelles, P. Ring, and P. Schuck, Phys. Rev. C **84**, 054309 (2011).
[27] P. W. Zhao, Z. P. Li, J. M. Yao, and J. Meng, Phys. Rev. C **82**, 054319 (2010).
[28] Q. S. Zhang, Z. M. Niu, Z. P. Li, J. M. Yao, and J. Meng, Frontiers Phys. **9**, 529 (2014).
[29] G. A. Lalazissis, J. König, and P. Ring, Phys. Rev. C **55**, 540 (1997).
[30] J. D. Walecka, Ann. Phys. (NY) **83**, 491 (1974).
[31] A. Akmal, V. R. Pandharipande, and D. G. Ravenhall, Phys. Rev. C **58**, 1804 (1998).
[32] M. Baldo, P. Schuck, and X. Viñas, Phys. Lett. B **663**, 390 (2008).
[33] E. N. E. van Dalen, C. Fuchs, and A. Faessler, Eur. Phys. J. A **31**, 29 (2007).
[34] P. Manakos and T. Mannel, Z. Phys. A **330**, 223 (1988).
[35] J. M. Yao, K. Hagino, Z. P. Li, J. Meng, and P. Ring, Phys. Rev. C **89**, 054306 (2014).
[36] S. Brandt, *Data Analysis: Statistical and Computational Methods for Scientists and Engineers* (Springer, Switzerland, 2014).
[37] M. Warda and J. L. Egido, Phys. Rev. C **86**, 014322 (2012).
[38] B.-N. Lu, J. Zhao, E.-G. Zhao, and S.-G. Zhou, Phys. Rev. C **89**, 014323 (2014).
[39] T. Bürvenich, M. Bender, J. A. Maruhn, and P.-G. Reinhard, Phys. Rev. C **69**, 014307 (2004).
[40] A. Staszczak, A. Baran, and W. Nazarewicz, Phys. Rev. C **87**, 024320 (2013).
[41] A. V. Afanasjev and O. Abdurazakov, Phys. Rev. C **88**, 014320 (2013).
[42] W. Pannert, P. Ring, and J. Boguta, Phys. Rev. Lett. **59**, 2420 (1987).
[43] Y. K. Gambhir, P. Ring, and A. Thimet, Ann. Phys. (NY) **198**, 132 (1990).
[44] P. Ring, Y. K. Gambhir, and G. A. Lalazissis, Comput. Phys. Commun. **105**, 77 (1997).
[45] T. Nikšić, N. Paar, D. Vretenar, and P. Ring, Comput. Phys. Commun. **185**, 1808 (2014).
[46] S. E. Agbemava and A. V. Afanasjev, (unpublished).
[47] Y. Tian, Z. Y. Ma, and P. Ring, Phys. Lett. B **676**, 44 (2009).
[48] J. Dobaczewski, A. V. Afanasjev, M. Bender, L. M. Robledo, and Y. Shi, Nucl. Phys. A **944**, 388 (2015).
[49] A. V. Afanasjev, T. L. Khoo, S. Frauendorf, G. A. Lalazissis, and I. Ahmad, Phys. Rev. C **67**, 024309 (2003).
[50] A. V. Afanasjev, P. Ring, and J. König, Nucl. Phys. A **676**, 196 (2000).
[51] H. Abusara, A. V. Afanasjev, and P. Ring, Phys. Rev. C **82**, 044303 (2010).
[52] B.-N. Lu, E.-G. Zhao, and S.-G. Zhou, Phys. Rev. C **85**, 011301 (2012).
[53] R. T. Birge, Phys. Rev. **40**, 207 (1932).
[54] R. Sheline, I. Ragnarsson, and S. Nilsson, Phys. Lett. B **41**, 115 (1972).
[55] A. V. Afanasjev and H. Abusara, Phys. Rev. C **78**, 014315 (2008).
[56] J. D. McDonnell, N. Schunck, D. Higdon, J. Sarich, S. M. Wild, and W. Nazarewicz, Phys. Rev. Lett. **114**, 122501 (2015).
[57] V. Prassa, T. Nikšić, and D. Vretenar, Phys. Rev. C **88**, 044324 (2013).
[58] A. V. Afanasjev, H. Abusara, and P. Ring, Eur. Phys. J. Web Conf. **62**, 03003 (2013).
[59] P. Möller, A. J. Sierk, T. Ichikawa, A. Iwamoto, R. Bengtsson, H. Uhrenholt, and S. Åberg, Phys. Rev. C **79**, 064304 (2009).
[60] M. Kowal, P. Jachimowicz, and A. Sobiczewski, Phys. Rev. C **82**, 014303 (2010).
[61] P. Möller and J. Nix, Nucl. Phys. A **536**, 20 (1992).
[62] S. Karatzikos, A. V. Afanasjev, G. A. Lalazissis, and P. Ring, Phys. Lett. B **689**, 72 (2010).
[63] P. Ring and P. Schuck, *The Nuclear Many-Body Problem* (Springer-Verlag, Berlin, 1980).
[64] N. Schunck and L. M. Robledo, Rep. Prog. Phys. **79**, 116301 (2016).
[65] R. Rodríguez-Guzmán and L. M. Robledo, Phys. Rev. C **89**, 054310 (2014).
[66] S. Goriely, A. Bauswein, and H.-T. Janka, Astrophys. J. **738**, L32 (2011).
[67] M. Bender, K. Rutz, P.-G. Reinhard, J. A. Maruhn, and W. Greiner, Phys. Rev. C **60**, 034304 (1999).